An Experimental and Theoretical Investigation into the Formation of Ketene (H_2CCO) and Ethynol (HCCOH) in Interstellar Analog Ices

Andrew M. Turner[1,2], Andreas S. Koutsogiannis[2], N. Fabian Kleimeier[1,2], Alexandre Bergantini[1,2] , Cheng Zhu[1,2], Ryan C. Fortenberry[3] , and Ralf I. Kaiser[1,2]

[1] Department of Chemistry, University of Hawaii at Manoa, Honolulu, HI 96822, USA
[2] W. M. Keck Laboratory in Astrochemistry, University of Hawaii at Manoa, Honolulu, HI 96822, USA
[3] Department of Chemistry & Biochemistry, University of Mississippi, University, MS 38677, USA
Received 2020 March 10; revised 2020 April 21; accepted 2020 April 25; published 2020 June 16

Abstract

The formation of isomers of C_2H_2O—ketene (H_2CCO), ethynol (HCCOH), and oxirene (c-CHCHO)—was investigated in interstellar ice analogs composed of carbon monoxide and water. Using tunable photoionization time-of-flight mass spectrometry to selectively ionize the isomer of interest, ketene and ethynol were detected as reaction products, but oxirene remains elusive. These findings demonstrate that organic compounds that are precursors to complex organic molecules can form without an organic source of carbon. Furthermore, we report the first plausible detection of ethynol in astrophysically relevant ices. These investigations were supported by theoretical calculations describing reaction energies, pathways, ionization energies, and harmonic frequencies.

Unified Astronomy Thesaurus concepts: Laboratory astrophysics (2004); Interdisciplinary astronomy (804); Chemical abundances (224); Interstellar molecules (849); Astrochemistry (75)
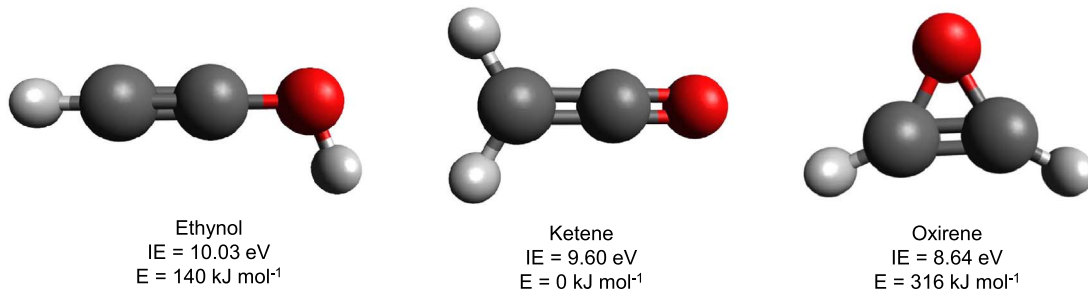
1. Introduction

Fundamental knowledge of the formation of structural isomers—molecules with the same molecular formula but different connectivities of atoms—of complex organic molecules (COMs) is of crucial importance as these molecules are regarded as tracers to the physical and chemical conditions of interstellar environments and to test chemical models of molecular clouds and star-forming regions. The unraveling of the formation routes to distinct isomers of C_2H_4O [acetaldehyde (HCOCH₃), vinyl alcohol (C_2H_3OH), ethylene oxide (c-C_2H_4O)], $C_2H_4O_2$ [acetic acid (CH₃COOH), methyl formate (HC(O)OCH₃), glycolaldehyde (HC(O)CH₂OH)], and C_3H_6O [acetone (CH₃C(O)CH₃), propanal (HC(O)C₂H₅), propylene oxide (c-C_3H_6O)] within icy grains has just scratched the surface (Figure 1) (Bennett et al. 2005; Bennett & Kaiser 2007; Abplanalp et al. 2016; Bergantini et al. 2018a, 2018b). For instance, considering the $C_2H_4O_2$ system, all isomers were detected toward the hot core Sgr B2 (Fourikis et al. 1974; Dickens et al. 1997; Turner & Apponi 2001), but only methyl formate was observed in molecular clouds such as OMC-1 (Hollis et al. 2003). Consequently, despite the key role of structural isomers as tracers to define the evolutionary stage of molecular clouds and star-forming regions, together with their chemical and physical boundary conditions, no comprehensive evidence has been given so far on their formation mechanism. Models of gas-phase-only chemistry yield a factor of up to 100 less than observed. Mehringer & Snyder (1996) proposed that COMs are initially formed on interstellar grains in molecular clouds at 10 K and then injected into the gas phase in star-forming regions once the temperature of the grains increases and hence the molecules sublime. Charnley et al. (1992) and Caselli et al. (1993) extended previous models and injected COMs, formed inside interstellar ice-coated grains at 10 K and/or on their surfaces at temperatures exceeding 40 K via radical diffusion and recombination, to simulate these grain sublimation processes. However, even these refined models did not fit observed abundances of isomers such as of acetic acid,

glycolaldehyde, and methyl formate simultaneously. These models suggest that key production routes to COMs on interstellar grains are missing. It is crucial to point out that previous astrochemical models simulating the formation of COMs on interstellar grains have postulated that the ice mantle is predominantly inert and that only the ice surface takes part in the synthesis of new molecules. This has limited the validity of astrochemical models since an interaction of ionizing radiation with ices can lead to the formation of COMs. In combined laboratory and astrochemical modeling studies, Kaiser and Herbst provided compelling evidence that COMs, specifically the isomer pairs acetaldehyde–vinyl alcohol (CH₃CHO–C_2H_3OH) (Abplanalp et al. 2016) and propylene oxide–acetone (c-C_3H_6O–CH₃C(O)CH₃) (Bergantini et al. 2018a), can be synthesized within interstellar ices via processing by Galactic cosmic-rays (GCRs). However, considering that about one third of all detected interstellar molecules can be classified as COMs, these studies only scratched the surface. A comprehensive incorporation of these processes into astrochemical models simulating the formation of COMs in molecular clouds and star-forming regions is still in its infancy, since laboratory data on rate constants, reaction products, and their branching ratios and their dependence on the temperature and chemical composition of the ices are still sparse.

This is in particular true for the C_2H_2O isomers ketene (H_2CCO), ethynol (HCCOH), and oxirene (c-CHCHO) as potential reactants toward larger organic molecules both in laboratories and the interstellar medium (Zasimov et al. 2020) (Figure 2). Ketene (H_2CCO) contains an alkene and carbonyl functional group while ethynol, also called hydroxyacetylene, carries a carbon–carbon triple bond and a hydroxyl group but is less stable by 140 kJ mol^{-1} with respect to ketene. The elusive oxirene represents an epoxide and has neither been observed in any laboratory nor in deep space (Tanaka & Yoshimine 1980; Scott et al. 1994; Vacek et al. 1994), which is consistent with the minimum energy principle described by Shingledecker et al. (2019) in their search for isomers of C_3H_2O. Among these isomers, only ketene has thus far been observed in the interstellar medium. Ketene was first detected toward Sgr B2
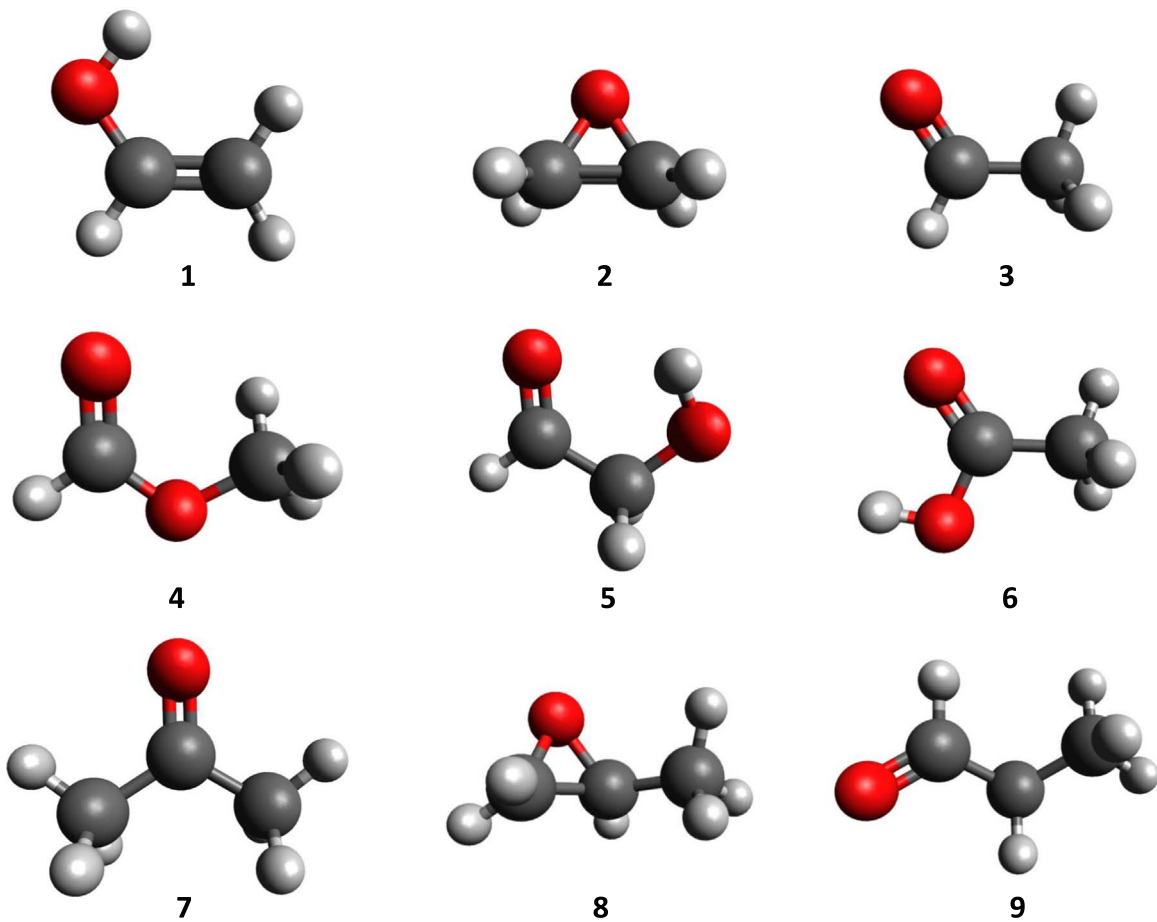
Figure 1. Isomers of C_2H_4O (top, (1) vinyl alcohol, (2) ethylene oxide, (3) acetaldehyde), $C_2H_4O_2$ (center, (4) methyl formate, (5) glycolaldehyde, (6) acetic acid), and C_3H_6O (bottom, (7) acetone, (8) propylene oxide, (9) propanal).

Ethynol
IE = 10.03 eV
E = 140 kJ mol⁻¹

Ketene
IE = 9.60 eV
E = 0 kJ mol⁻¹

Oxirene
IE = 8.64 eV
E = 316 kJ mol⁻¹

Figure 2. Isomers of C_2H_2O along with their calculated ionization and relative energies as determined by this study.

(Turner 1977) with a fractional abundance (f (H_2)) of 2.0×10^{-10} compared to molecular hydrogen (Nummelin et al. 2000), and later toward Orion KL (f (H_2) $= 3 \times 10^{-7}$; Johansson et al. 1984), TMC-1 (f (H_2) $= 4 \times 10^{-11}$; Matthews & Sears 1986; Irvine et al. 1989; Ohishi et al. 1991), and the translucent clouds CB 17, CB 24, and CB 228 (f (H_2) $= 1.1 \times 10^{-9}$; Turner et al. 1999). In addition, ketene has been found with f (H_2) $\sim 10^{-10}$ toward protostars AFGL 989, WL 22, NGC 6334I, and NGC 7538 I1 (Ruiterkamp et al. 2007) as well as the prestellar core L1269B (Bacmann et al. 2012) and the PKS 1830–211 galaxy (Muller et al. 2011). It is perhaps surprising that ethynol (HCCOH) has not yet been detected given the interstellar observation of the ethynyl radical (HCC) (Tucker et al. 1974) and the ketenyl radical (HCCO) (Agúndez et al. 2015). Thus, an experimental and

computational exploration of the potential formation of C_2H_2O isomers in interstellar ices is pertinent to constrain the potential for ethynol, which is not yet found in the interstellar medium, and oxirene, which has remained elusive under any conditions, to form in interstellar space.

Several studies have exclusively focused on the formation of ketene in interstellar ice analogs. Hudson & Loeffler (2013) utilized infrared spectroscopy to identify ketene in proton-irradiated binary ice mixtures including carbon dioxide (CO_2), acetylene (C_2H_2), molecular oxygen (O_2), water (H_2O), ethylene (C_2H_4), carbon monoxide (CO), and methane (CH_4). The 0.8 MeV protons simulate the effect of GCRs by generating lower-energy secondary electrons that process the ice. Proposed pathways toward ketene include the addition of atomic oxygen (O), which is sourced from CO_2 or O_2, to C_2H_2.

In ices with water, the suggested pathway instead dissociates water into a hydrogen atom (H) and hydroxyl radical (OH), which then both add to acetylene to form vinyl alcohol (C_2H_3OH). The decomposition of vinyl alcohol by molecular hydrogen (H_2) elimination then produces ketene. These pathways were proposed based on a comparison of the chemical structure of the reactants and products. Under similar experimental conditions, Hudson (2018) later observed ketene in irradiated pure ices of acetone (CH_3COCH_3) and acetic acid (CH_3COOH) and proposed a formation route through cleavage of the methyl radical (CH_3) followed by hydrogen loss, possibly through abstraction by the lost methyl radical. The interaction of oxygen with two-carbon hydrocarbon ices (ethane (C_2H_6), ethylene (C_2H_4), and acetylene (C_2H_2)) was further investigated by Bergner et al. (2019) using atomic oxygen—presumed to be in the excited state. Ketene was detected in each ice but was a major product only in the acetylene ices. Acetylene ices were further studied by Chuang et al. (2020) in mixtures with molecular oxygen (O_2) that were subjected to an atomic hydrogen beam source. Atomic hydrogen reacts to eventually form the hydroxyl radical (OH), which was proposed to react with acetylene to form the hydroxyvinyl radical (CHCHOH). The inferred reaction proceeds via isomerization to the acetyl radical (CH_3CO) before forming ketene by hydrogen atom loss. Reactions with atomic hydrogen were also considered by Haupa et al. (2020) in which acetamide ($CH_3C(O)NH_2$) was condensed in a para-hydrogen (p-H_2) matrix along with molecular chlorine (Cl_2). Irradiation with ultraviolet (UV) and infrared light produced atomic hydrogen that abstracted a hydrogen from acetamide to form the $CH_2C(O)NH_2$ radical. Further photolysis with 380–445 nm photons cleaved the amino (NH_2) group to form ketene.

Maity et al. (2014) exposed ices of methane and carbon monoxide to energetic electrons and utilized photoionization coupled with reflectron time-of-flight mass spectrometry (ReTOF-MS) to detect subliming reaction products. Kinetic fitting of the temporal profiles of the reactants, intermediates, and products using coupled differential equations revealed that carbon monoxide is electronically excited and dissociates to atomic carbon and oxygen, and the carbon subsequently reacts with another carbon monoxide molecule to form dicarbon monoxide (CCO; $X^3\Pi$) followed by hydrogenation to ketene (H_2CCO). In principle, hydrogenation of dicarbon monoxide (CCO; $X^3\Pi$) at both the carbon and oxygen atoms could also lead to ethynol (HCCOH). In a follow up study, Zasimov et al. (2020) considered acetylene–water (C_2H_2–H_2O) ices but, unlike Hudson & Loeffler (2013), who utilized a 5:1 water-rich ice with acetylene, this study considered a 1:1 mixture in noble gas matrices and processed the ices using X-rays. Infrared spectroscopy confirmed the formation of ketene as well as the weakly bound H_2CCO–H_2 complexes, which likely results from the photoinduced intermolecular oxygen transfer from the C_2H_2–H_2O complex similar to those observed with HCCO–CO complexes (Ryazantsev et al. 2017). The ketenyl radical (HCCO) was also observed after atomic hydrogen elimination from ketene. Further, Abplanalp & Kaiser (2019) also detected ketene in ice mixtures of carbon monoxide with ethane (C_2H_6), ethylene (C_2H_4), and acetylene (C_2H_2) exposed to ionizing radiation.

While ketene is a common laboratory reagent, ethynol was not experimentally detected until 1986 as a decarbonylation product of the propiolic acid cation ($HCCCOOH^+$) followed by charge neutralization (van Baar et al. 1986). This study notes a high isomerization barrier to ketene close to $300\,kJ\,mol^{-1}$ concluding that once formed, ethynol should be kinetically stable. In laboratory ices, Dommen et al. (1987) unsuccessfully attempted to produce ethynol from propiolic acid in an argon matrix, but Hochstrasser & Wirz (1989) generated ethynol by the irradiation of 3-hydroxy-cyclobutene-1,2-dione (semisquaric acid) in argon and proposed that the UV photolysis of ketene converts ketene to ethynol in an argon matrix (Hochstrasser & Wirz 1990). Given that ethynol (HCCOH) is a stable isomer of ketene and the plausible formation of ethynol from hydrogenation at the carbon and oxygen atom of dicarbon monoxide (CCO; $X^3\Pi$), it is surprising that ethynol has not yet been detected in astrophysically relevant ices.

Here, we present our results from interstellar ice analogs of carbon monoxide and water (CO–H_2O) exposed to ionizing radiation in the form of energetic electrons. Like high-energy protons, energetic electrons produce a cascade of secondary electrons that simulate the irradiation of interstellar ices by GCRs (Bennett et al. 2011). In the search for the C_2H_2O isomers, CO–H_2O ices are unique since they do not contain an organic source of carbon like C_2H_2 or CH_4. Thus CO–H_2O ices would examine the potential formation of C_2H_2O isomers in water-rich environments. In addition, water and carbon monoxide are excellent choices for interstellar ice analogs, as water is the most abundant molecule in interstellar ices, and the fractional abundance of carbon monoxide compared to water is about $f(H_2O) = 0.1$ (Öberg et al. 2011; Bouilloud et al. 2015). These experiments are combined with high-level quantum chemical calculations and provide compelling evidence of the formation of two distinct isomers in the processed water–carbon monoxide ices: ketene (H_2CCO) and ethynol (HCCOH), thus paving the way for future astronomical detection of the hitherto elusive interstellar ethynol molecule (HCCOH).

2. Experimental

Experiments were conducted in a stainless steel chamber capable of reaching ultrahigh vacuum pressures down to 10^{-11} Torr (Jones & Kaiser 2013). Carbon monoxide (Sigma Aldrich, >99%) was premixed with water vapor (H_2O) obtained from an evacuated vial of HPLC-grade water (Fisher Scientific) to prepare a 10 Torr CO to 20 Torr H_2O gas mixture. This mixture passed into the main chamber via a glass capillary array and was deposited onto a polished silver substrate, which was mounted on an oxygen-free high-conductivity copper cold finger cooled to 5 K using a closed-cycle helium refrigerator (Sumitomo Heavy Industries, RDK-415E). The ice thickness was determined using laser interferometry (Turner et al. 2015) and found to be $750 \pm 50\,nm$, and CASINO calculates an average electron penetration depth of $280 \pm 30\,nm$ (Hovington et al. 1997). Fourier transform infrared spectra (Nicolet 6700, $4\,cm^{-1}$ resolution) of the deposited ices revealed a condensed CO-to-H_2O ratio of $1.0 \pm 0.1 : 1$ by utilizing the following bands and their absorption coefficients: $2138\,cm^{-1}$ (ν_1, CO, $1.1 \times 10^{-17}\,cm\,molecule^{-1}$), $2090\,cm^{-1}$ (ν_1, ^{13}CO, $1.3 \times 10^{-17}\,cm\,molecule^{-1}$), $1660\,cm^{-1}$ (ν_2, H_2O, $9.8 \times 10^{-17}\,cm\,molecule^{-1}$), and $3300\,cm^{-1}$ (ν_1/ν_3, H_2O, $3.8 \times 10^{-16}\,cm\,molecule^{-1}$) (Bouilloud et al. 2015; Turner et al. 2018a). The ice mixture was irradiated with 5 keV electrons for 2 hr at a current of 50 nA, which results in a dose of $10 \pm 2\,eV$

Table 1
Parameters for the Vacuum Ultraviolet Light Generation Used in the Present Experiments

ω_1 (nm)	ω_2 (nm)	Nonlinear Medium	Four-wave Mixing Scheme[a]	ω_{VUV} (nm)	ω_{VUV} (eV)
202.2	611.8	Krypton	$2\omega_1 - \omega_2 = \omega_{\text{VUV}}$	121.2	10.23
202.2	494.7	Krypton	$2\omega_1 - \omega_2 = \omega_{\text{VUV}}$	127.2	9.75
222.4	607.4	Xenon	$2\omega_1 - \omega_2 = \omega_{\text{VUV}}$	136.2	9.10

Note.
[a] Frequencies are used for four-wave mixing equations.

molecule^{-1} for water and 15 ± 3 eV molecule^{-1} for CO. For an interstellar ice grain, these doses are equivalent to approximately 5×10^6 yr, which is a typical lifetime for a molecular cloud (Strazzulla et al. 1991). After irradiation, a temperature-programmed desorption (TPD) scheme heated the ice from 5 to 300 K at 1 K minutes^{-1}. The subliming molecules were photoionized and detected using ReTOF-MS (Jordon TOF Products, Inc). Considering the ionization energies of the target molecules of 10.03 eV (ethynol), 9.60 eV (ketene), and 8.64 eV (oxirene) (see Figure 2 and Section 3), three photon energies were chosen in order to distinguish between the isomers of C_2H_2O based on their ionization energies. The highest photon energy, 10.23 eV, is capable of ionizing all isomers, while 9.75 eV was chosen to ionize only ketene and oxirene. A third photon energy of 9.10 eV was utilized to ionize oxirene if present. The photons were produced using two pulsed Nd:YAG lasers (neodymium-doped yttrium aluminum garnet, Spectra Physics, PRO-250, 30 Hz) that each pumped a dye laser and the outputs were combined via four-wave mixing ($\omega_{\text{vuv}} = 2\omega_1 - \omega_2$) to produce the desired vacuum ultraviolet (VUV) photon (Jones & Kaiser 2013). Krypton and xenon were utilized as the nonlinear medium necessary for four-wave mixing (Table 1). The VUV photons were separated from other photon energies using a lithium fluoride lens and passed 1 mm above the ice surface to ionize subliming molecules. The ReTOF-MS correlates the arrival times of the ionized molecules to mass-to-charge ratios using an amplified signal from a fast preamplifier (Ortec 9305) and 4 ns bin width that is triggered at 30 Hz (Quantum Composers, 9518). To confirm the mass assignments, the experiments at 10.23 eV were repeated using isotopically labeled D2-water (D$_2$O, 99.9 atom% D) and ^{13}CO (99 atom% ^{13}C). An additional experiment without electron irradiation was performed that verified an external energy source was necessary to produce the observed signals (blank).

3. Theoretical

Quantum chemical explorations of reaction schemes for comparison to astrochemical models or observations are a common augmentation to laboratory astrochemical studies (Rimola et al. 2012; Shivani et al. 2017; Krim et al. 2019; Zhao et al. 2020). In the present study, the minimum energy geometries are optimized and harmonic frequencies computed with the CCSD(T) method (Raghavachari et al. 1989) and the aug-cc-pVTZ basis set (Kendall et al. 1992; Peterson & Dunning 1995). Subsequent CCSD(T)/aug-cc-pVQZ computations at these geometries are utilized with a two-point complete basis set (CBS) limit extrapolation (Martin & Lee 1996) to produce more accurate energies. The energy at

each minimum is corrected for harmonic zero-point vibrational energies (ZPVEs) from the CCSD(T)/aug-cc-pVTZ harmonic frequencies. The optimized transition states are determined from B3LYP (Yang et al. 1986; Lee et al. 1988; Becke 1993) again with the aug-cc-pVTZ basis set followed by vibrational frequency computations. Then, CCSD(T)/aug-cc-pVTZ/QZ single-point energies provide CBS extrapolated energies for the transition states further energy-corrected via B3LYP/aug-cc-pVTZ ZPVEs. All relative energies are determined with respect to the $CCO(X^3\Pi)/2H$ reactants with the CCSD(T)/CBS + ZPVE energies at each point. Relaxed potential energy scans at the CCSD(T)/aug-cc-pVTZ level of theory utilize 0.1 Å step sizes for the C/O–H coordinate in question while the other structural parameters are allowed to optimize. All coupled cluster computations are done with the Molpro2015.1 quantum chemistry program (Werner et al. 2012, 2015), and all B3LYP computations utilize the Gaussian09 quantum chemistry program (Frisch et al. 2009). Coordinates and harmonic frequencies are provided in the Appendix, Tables A1 and A2.

4. Results

Based on infrared spectroscopy, the dominant irradiation product is carbon dioxide (CO$_2$, 2341 cm^{-1}; ^{13}CO$_2$, 2279 cm^{-1}) (Turner et al. 2015), which is expected from CO-containing ices, along with formaldehyde (H$_2$CO); 1711 cm^{-1} (v_2), 2723 cm^{-1} (v_2+v_4), 2835 cm^{-1} (v_1), and 2936 cm^{-1} (v_5) (Figure 3) (Butscher et al. 2016). The formyl radical (HCO) is seen at 1845 cm^{-1} (v_3). Previous studies of irradiated H$_2$O/CO ices found that formyl radicals (HCO) combine with hydroxyl radicals (OH) to form formic acid (H$_2$CO$_2$), while an additional minor pathway involving the hydroxylcarbonyl radical (HOCO) combining with a hydrogen atom also led to formic acid (Bennett et al. 2011). However, neither formic acid nor the HOCO radical were spectroscopically observed in the present study. The intense v_2 band of ketene (H$_2$CCO, 2131 cm^{-1}) is obscured by the carbon monoxide fundamental at 2138 cm^{-1} (Maity et al. 2014). Thus, the infrared detection of ketene was pursued by exploiting isotopic shifts in the H$_2$O/^{13}CO, D$_2$O/CO, and D$_2$O/^{13}CO irradiated ices. In these infrared spectra, the corresponding ketene bands (H$_2^{13}$C^{13}CO at 2071 cm^{-1}, D$_2$CCO at 2109 cm^{-1}, and D$_2^{13}$C^{13}CO at 2107 cm^{-1}) (Maity et al. 2014) were not observed despite their separation from overlapping bands suggesting low concentrations of ketene formed. In addition, the v_3 band of ethynol (HCCOH), which was observed at 2198 cm^{-1} in matrix isolation (Hochstrasser & Wirz 1990), was not detected in the H$_2$O–CO irradiated ice. Since the infrared absorption bands of the C$_2$H$_2$O products of interest are low intensity or overlap with other bands, the primary utility of the infrared spectra was to monitor the reactants. The intensity decrease for the reactant absorption bands indicate that $13\% \pm 3\%$ of water and $15\% \pm 2\%$ of carbon monoxide reacted during the irradiation. This equates to $1.2 \pm 0.3 \times 10^{17}$ molecules of water and $1.4 \pm 0.2 \times 10^{17}$ molecules of carbon monoxide reacted; thus, $7.0 \pm 0.3 \times 10^{16}$ molecules serve as the theoretical upper limit for any C$_2$H$_2$O products formed.

Reflectron time-of-flight mass spectrometry proved to be a more powerful tool for the identification of C$_2$H$_2$O isomers. At 10.23 eV, the TPD profiles for $m/z = 42$ (C$_2$H$_2$O$^+$) reveal multiple distinct absorption events (Figure 4). The first event has an onset sublimation temperature of 80 K that peaks between 95 and 100 K while a second, stronger peak arises at 130 K and peaks around 155 K. This second peak transitions to
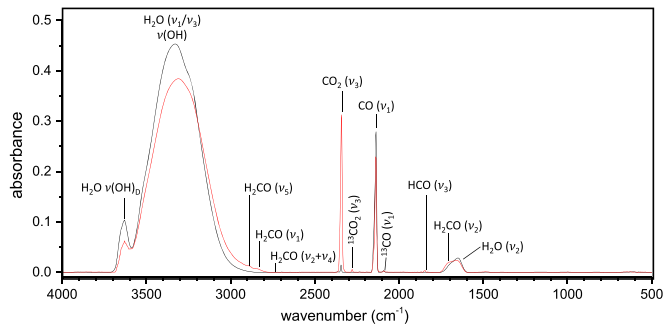
Figure 3. Infrared spectrum of pristine (black) and irradiated (red) CO–H_2O ice.
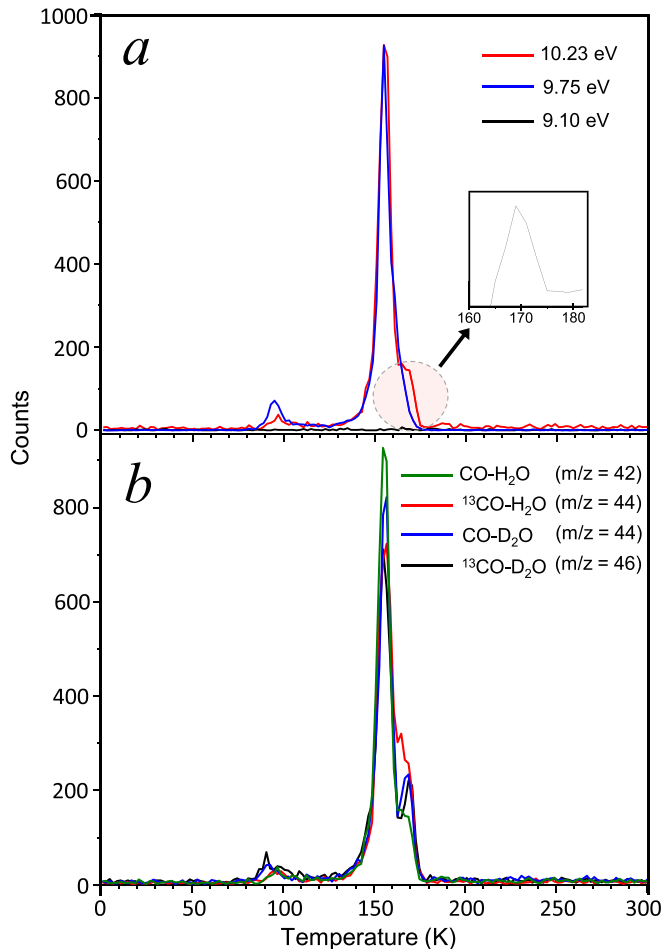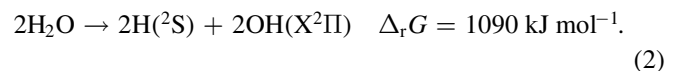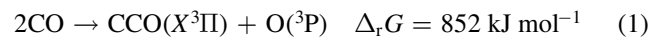

Figure 4. (a) TPD profiles for C_2H_2O ($m/z = 42$) in CO–H_2O ice at 10.23 eV (red), 9.75 eV (blue), and 9.10 eV (black). The circled area indicates the ethynol sublimation while the inset shows the difference spectrum to elucidate the sublimation peak. (b) TPD profiles at 10.23 eV for isotopically labeled CO–H_2O ice mixtures.

a less intense third peak before returning to baseline at 175 K. The assignment of this signal to C_2H_2O is confirmed by matching profiles for the isotopically labeled ices of D_2O–CO ($D_2C_2O^+$, $m/z = 44$), H_2O–^{13}CO ($H_2^{13}C_2O^+$, $m/z = 44$), and D_2O–^{13}CO ($D_2^{13}C_2O^+$, $m/z = 46$). These profiles differ from results by Abplanalp & Kaiser (2019) of irradiated carbon monoxide–methane (CO–CH_4) ices that showed only a single sublimation event for $m/z = 42$ peaking near 100 K, which is consistent with our lower-temperature sublimation peak. We attribute our more intense higher-temperature sublimation peak

to the water matrix trapping the C_2H_2O molecules until water begins to recrystallize or sublime. In order to distinguish between the C_2H_2O isomers, experiments were conducted at distinct photon energies. The ionization energy for each of the three isomers of interest was calculated (Figure 2) with the computed value of ketene (9.60 eV) being in excellent agreement with the experimental data (9.60–9.61 eV) (Bock & Mohmand 1977; Vogt et al. 1978). As ethynol (HCCOH) is the highest calculated ionization energy (IE = 10.03 eV), 10.23 eV was chosen to photoionize all isomers. The proceeding experiments then used 9.75 eV as an intermediate value between ethynol and ketene (H_2CCO; IE = 9.60 eV) and finally 9.10 eV, which is above the 8.64 eV calculated ionization energy of oxirene (c-CHCHO). The absence of signal at 9.10 eV eliminates the elusive oxirene molecule (IE = 8.64 eV) as a potential product. However, the profile at 9.75 eV is similar to 10.23 eV; in particular, the major sublimation event peaking at 155 K is present in both experiments. Thus, the detection of ketene (IE = 9.60 eV) is confirmed. The detection of ethynol (IE = 10.03 eV) would be confirmed by the absence of a distinct signal at 9.75 eV that is present at 10.23 eV. In this case, the best candidate for ethynol is the second sublimation event that remains between 165 and 175 K. This event is present at 10.23 eV in all isotopic experiments and is more clearly seen when D_2O is substituted for H_2O. In H_2O ices, this peak is less resolved and appears as a shoulder to the more intense peak assigned to ketene. At 9.75 eV, this smaller peak is not observed, and the ketene desorption profile returns to baseline without the shoulder. It should be stressed that these ion counts are not present in the blank experiments, i.e., in experiments conducted without subjecting the ices to ionizing radiation. Therefore, these ion counts are connected with radiolyzed ice samples.

5. Discussion

Ketene is a widely studied and observed isomer of C_2H_2O, but our detection of ethynol (HCCOH) is notable as the first identification in astrophysical ice analogs. Based on accompanying quantum chemical calculations and previous experimental studies of carbon monoxide ices in our laboratory under identical irradiation conditions, we propose that the path toward the C_2H_2O isomers begins with two carbon monoxide molecules reacting to form dicarbon monoxide ($CCO(X^3\Pi)$, reaction (1)) and atomic oxygen (^3P) as shown by Maity et al. (2014). This reaction also represents the starting point in pure carbon monoxide ices (Jamieson et al. 2006). Likewise, water can be radiolyzed to a hydroxyl radical plus a hydrogen atom (reaction (2)) (Zheng et al. 2006a, 2006b, 2007). These processes are strongly endoergic by at least 852 kJ mol^{-1} as supplied from the impinging radiation.

$$2CO \rightarrow CCO(X^3\Pi) + O(^3P) \quad \Delta_r G = 852 \text{ kJ mol}^{-1} \quad (1)$$

$$2H_2O \rightarrow 2H(^2S) + 2OH(X^2\Pi) \quad \Delta_r G = 1090 \text{ kJ mol}^{-1}. \quad (2)$$

These reactants—dicarbon monoxide and two hydrogen atoms—represent the starting material to synthesize ketene and the ethynol isomers (Figure 5) with ketene representing the global minimum. First, ethynol can eventually form via successive, barrierless hydrogen atom additions involving, first, the reaction of dicarbon monoxide ($CCO(X^3\Pi)$) with atomic hydrogen forming intermediate i3 via addition to the oxygen
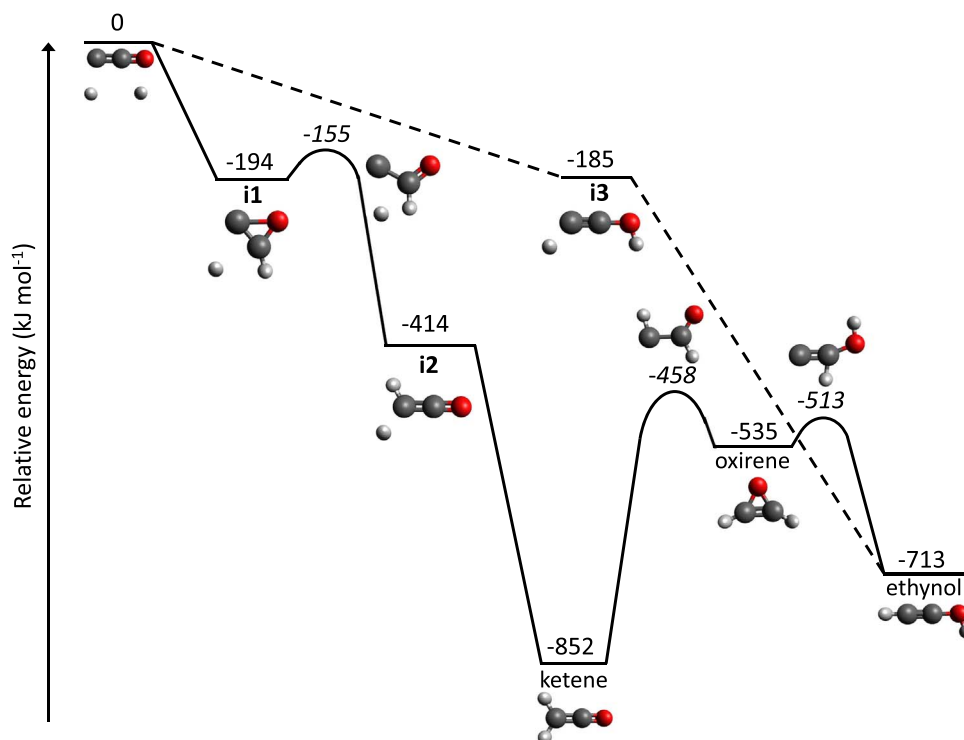
Figure 5. CCSD(T)/CBS reaction scheme with relative energies in kilojoules per mole showing the reactions from $2H + CCO$ ($X^3\Pi$) to ketene, oxirene, and ethynol.

atom; thereafter, i3 reacts then with another hydrogen atom through addition to the terminal carbon atom forming ethynol (dashed lines). Second, the formation of ketene is initiated by barrierless addition of atomic hydrogen to the central carbon atom of $CCO(X^3\Pi)$ leading to intermediate i1, which then isomerizes to the ketenyl (HCCO) intermediate i2. The calculations could not locate a one-step pathway for the addition of atomic hydrogen to dicarbon monoxide leading to ketenyl (HCCO) i2. The latter can react with a second hydrogen atom to form ketene. Note that oxirene, although not observed in our studies, might be present as an isomerization product of ketene/ethynol and vice versa thus facilitating the interconversion of ketene to ethynol and of ethynol to ketene. Although this potential energy surface and the energetics are computed for gas-phase reactions, it also provides insights into how the reactions progress regardless of phase. While barrier heights may be lowered in the presence of water molecules like in these simulated interstellar ices (Woon 2004), the qualitative results of ketene being the minimum with ethynol lying above does not change. Furthermore, the lowering of barriers would further reduce the likelihood of oxirene existing long enough to be detected during any possible ethynol–ketene isomerization.

6. Astrophysical Implications

Our experiments demonstrated the facile synthesis of ketene and ethynol in interstellar ice analogs of carbon monoxide and water. These components are appropriate for simple astrophysical ice analogs as both are highly prominent interstellar ice constituents with carbon monoxide being abundant at levels of f (H_2O) = 0.1 compared to water. Unlike previous experiments, no organic carbon was initially present in the

ices, which indicates that ketene can be formed in interstellar ices of water, carbon monoxide, or carbon dioxide (CO_2), which can be radiolyzed to carbon monoxide (Turner et al. 2018a, 2018b), without the need for hydrocarbons such as methane (Figure 6). As ketene might represent a viable precursor toward COMs such as acetic acid (CH_3COOH) (Hudson & Loeffler 2013), these experiments demonstrate that complex astrochemical molecules might be formed via nonequilibrium chemistry without the initial presence of organic molecules. Also, ethynol has been previously formed in matrix isolation studies (Hochstrasser & Wirz 1989, 1990), but we report the first detection in interstellar ice analogs. While ketene's formation pathway is energetically favorable (Figure 5), our studies also provide feasible routes toward ethynol formation, thus ethynol is likely to exist in the ISM where ketene has been observed if the initial ices contain water and carbon monoxide (Figure 6). These routes may occur either via UV- or GCR-induced isomerization of ketene in a nonreactive environment analogous to the UV irradiation of ketene in matrix isolation (Hochstrasser & Wirz 1990) by a UV photon capable of overcoming the 4 eV ionization barrier (310 nm) or by GCR-initiated nonequilibrium chemistry of reactants such as carbon monoxide and water through chemistry as described in the present work. However, while oxirene may be an isomerization product of ketene or ethynol, our study suggests that any potential detection of oxirene in the ISM is doubtful and thus far experiments have supported this conclusion.

This also establishes an important connection between bulk interstellar ice chemistry—not simply ice surface processes—and gas-phase molecular detection as GCRs process the ices (simulated by high-energy electrons) to form products such as ketene deep within icy mantles that are not observed until the icy grains are heated and the products sublime. While our ketene production in interstellar ice analogs explains the
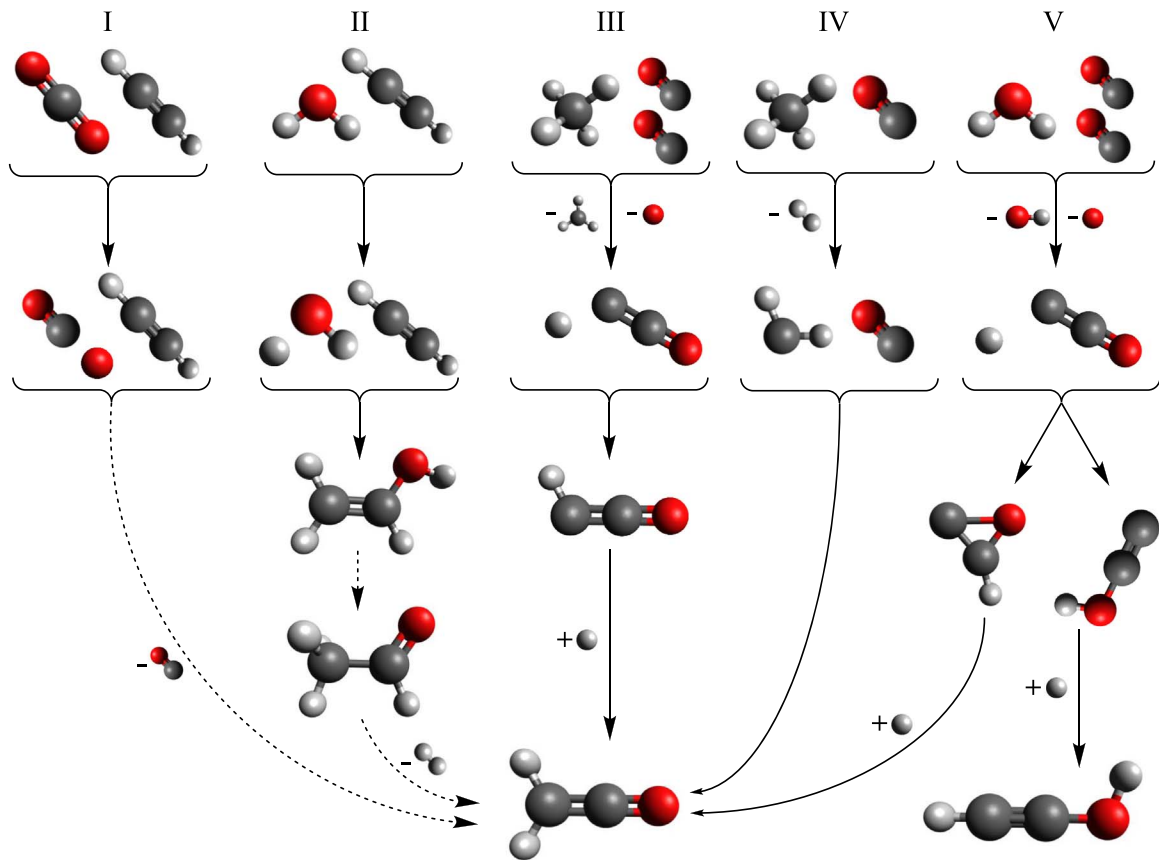
Figure 6. Reaction schemes showing pathways from ice mixtures of CO_2/C_2H_2 (I) (Hudson & Loeffler 2013), H_2O/C_2H_2 (II) (Hudson & Loeffler 2013), CH_4/CO (III, IV) (Maity et al. 2014), and H_2O/CO (V) (this work) to ketene and ethynol. All ice mixtures possess pathways whether hypothetical (dashed lines) or data-driven (solid lines) to ketene; only the H_2O/CO ice mixture has been shown to produce ethynol.

observed ketene detection in deep space, the detection of ethynol in the ice analogs provides evidence of its potential existence and prospective detection in the interstellar medium, thus providing astronomers a motivation to search for this missing isomer. The detection of interstellar ethynol would reinforce the interwoven relationship between laboratory astrochemistry and observational astronomy, as both rely on the discoveries of the other. As previous interstellar analog ice mixtures (CO_2–C_2H_2, H_2O–C_2H_2 (Hudson & Loeffler 2013), H_2O–CH_4 (Maity et al. 2014) (Figure 6)) that observed ketene failed to detect ethynol, the present work identifies ethynol as a tracer for a defined interstellar chemistry of water–carbon monoxide ices. Therefore, searches for ethynol should focus toward those regions were ketene has been detected (Sgr B2; Turner 1977, Orion KL; Johansson et al. 1984, TMC-1; Matthews & Sears 1986). If future astronomical searches identify ethynol,

our results provide a plausible indication of the interstellar chemistry as thus far ethynol has been found to form exclusively in water–carbon monoxide ices (Figure 6).

Appendix

Results for coordinates and harmonic frequencies from quantum chemical calculations (Section 3) are presented in Tables A1 and A2 below.

Table A1
Calculated Infrared Band Positions of Species in Figure 5

$^3\Pi$ CCO		^{2}A″ HCCO (i2)		^{2}A CCOH (i3)		^{2}A″ CCHO (i1)		CC(H)O TS	
Normal Modes	Position (cm^{-1})	Normal Modes	Position (cm^{-1})	Normal Modes	Position (cm^{-1})	Normal Modes	Position (cm^{-1})	Normal Modes	Position (cm^{-1})
ν_1 (σ)	2009.8	ν_1 (a')	3315.8	ν_1 (a)	3733.8	ν_1 (a')	3253.0	ν_1 (a)	2782.8
ν_2 (σ)	1068.3	ν_2 (a')	2047.4	ν_2 (a)	1956.0	ν_2 (a')	1522.7	ν_2 (a)	1429.4
ν_3 (π)	387.4	ν_3 (a')	1216.4	ν_3 (a)	1268.4	ν_3 (a')	1290.4	ν_3 (a)	1352.6
		ν_4 (a')	572.8	ν_4 (a)	1059.0	ν_4 (a')	1029.8	ν_4 (a)	997.5
		ν_5 (a')	516.1	ν_5 (a)	308.8	ν_5 (a'')	795.5	ν_5 (a)	767.9
		ν_6 (a'')	491.0	ν_6 (a)	157.9	ν_6 (a')	314.1	ν_6 (a)	443.3i

^{1}A$_1$ Ketene		^{1}A$_1$ Oxirene		^{1}A′ Ethynol		HCC(H)O TS		CC(H)OH TS	
Normal Modes	Position (cm^{-1})	Normal Modes	Position (cm^{-1})	Normal Modes	Position (cm^{-1})	Normal Modes	Position (cm^{-1})	Normal Modes	Position (cm^{-1})
ν_1 (b_2)	3297.3	ν_1 (a_1)	3394.8	ν_1 (a')	3798.2	ν_1 (a')	2981.1	ν_1 (a')	3795.8
ν_2 (a_1)	3192.4	ν_2 (b_2)	3322.0	ν_2 (a')	3474.0	ν_2 (a')	2962.2	ν_2 (a')	2730.1
ν_3 (a_1)	2181.0	ν_3 (a_1)	1756.6	ν_3 (a')	2230.4	ν_3 (a')	1704.5	ν_3 (a')	1893.3
ν_4 (a_1)	1411.3	ν_4 (a_1)	1063.0	ν_4 (a')	1270.2	ν_4 (a')	1401.0	ν_4 (a')	1318.3
ν_5 (a_1)	1148.4	ν_5 (b_2)	959.2	ν_5 (a')	1062.0	ν_5 (a')	1188.9	ν_5 (a')	1045.5
ν_6 (b_2)	989.6	ν_6 (a_1)	871.9	ν_6 (a')	610.3	ν_6 (a')	930.0	ν_6 (a')	843.5
ν_7 (b_1)	587.6	ν_7 (a_2)	589.6	ν_7 (a'')	527.3	ν_7 (a'')	849.0	ν_7 (a'')	535.2
ν_8 (b_1)	506.8	ν_8 (b_1)	505.2	ν_8 (a'')	378.4	ν_8 (a')	538.6	ν_8 (a'')	187.0
ν_9 (b_2)	434.5	ν_9 (b_2)	187.1	ν_9 (a')	355.0	ν_9 (a'')	920.3i	ν_9 (a')	242.2i

Table A2
Geometries Underlying the Calculated Energies for Species in Figure 5

Atom	X	Y	Z	Atom	X	Y	Z
	$^3\Pi$ CCO				^{2}A″ HCCO (i2)		
O	0.00000000	0.00000000	−1.111044266	O	0.00000000	0.0146297405	−1.147367824
C	0.00000000	0.00000000	0.0542336847	C	0.00000000	−0.068843393	0.0260279974
C	0.00000000	0.00000000	1.4257464693	C	0.00000000	0.1000200150	1.3231383628
				H	0.00000000	−0.603735808	2.1354044958
	^{2}A CCOH (i3)				^{2}A″ CCHO (i1)		
C	0.00000000	−0.003746363	−1.4124343372	H	0.00000000	1.7473081736	0.0752271481
C	0.00000000	−0.012029886	−0.2008734215	C	0.00000000	−0.415115878	−0.908118579
O	0.00000000	0.064131183	1.1177936734	C	0.00000000	0.6836632745	−0.107429805
H	0.00000000	−0.829981869	1.4816471138	O	0.00000000	−0.311680724	0.7576488614
	^{1}A$_1$ Ketene				^{1}A$_1$ Oxirene		
O	0.00000000	0.00000000	−1.1884211912	O	0.00000000	0.00000000	−0.858689927
C	0.00000000	0.00000000	−0.0210508033	C	0.00000000	−0.637526039	0.5020260765
C	0.00000000	0.00000000	1.2982946234	C	0.00000000	0.6375260387	0.5020260765
H	0.00000000	−0.942939836	1.8220581006	H	0.00000000	−1.655421685	0.8328140631
H	0.00000000	0.942939836	1.8220581006	H	0.00000000	1.6554216853	0.8328140631
	^{1}A′ Ethynol				CC(H)O TS		
H	0.00000000	0.0057285065	−2.4118740466	C	−0.018008	−0.130504	−0.015294
C	0.00000000	0.0034230373	−1.3501375509	C	0.104563	0.033105	1.358205
C	0.00000000	0.0113955214	−0.1422202250	O	0.861237	0.088892	−0.865046
O	0.00000000	−0.063755708	1.1752743341	H	−1.044365	−0.496961	−0.272611
H	0.00000000	0.8297055164	1.5398231963				
	HCC(H)O TS				CC(H)OH TS		
C	0.096828	0.428596	0.000000	C	0.000000	0.247200	0.000000
C	−1.343937	−0.072442	0.000000	C	1.026187	1.021565	0.000000
H	−1.224531	−1.171334	0.000000	O	−0.688460	−0.900113	0.000000
O	1.058472	−0.310767	0.000000	H	−0.071040	−1.641179	0.000000
H	0.239405	1.520541	0.000000	H	−0.578403	1.229495	0.000000

ORCID iDs

Alexandre Bergantini ⓘ https://orcid.org/0000-0003-2279-166X
Ryan C. Fortenberry ⓘ https://orcid.org/0000-0003-4716-8225
Ralf I. Kaiser ⓘ https://orcid.org/0000-0002-7233-7206

References

Abplanalp, M. J., Gozem, S., Krylov, A. I., et al. 2016, PNAS, 113, 7727
Abplanalp, M. J., & Kaiser, R. I. 2019, PCCP, 21, 16949
Agúndez, M., Cernicharo, J., & Guélin, M. 2015, A&A, 577, L5
Bacmann, A., Taquet, V., Faure, A., et al. 2012, A&A, 541, L12
Becke, A. D. 1993, JChPh, 98, 5648
Bennett, C. J., Hama, T., Kim, Y. S., et al. 2011, ApJ, 727, 27
Bennett, C. J., & Kaiser, R. I. 2007, ApJ, 661, 899
Bennett, C. J., Osamura, Y., Lebar, M. D., & Kaiser, R. I. 2005, ApJ, 634, 698
Bergantini, A., Abplanalp, M. J., Pokhilko, P., et al. 2018a, ApJ, 860, 108
Bergantini, A., Zhu, C., & Kaiser, R. I. 2018b, ApJ, 862, 140
Bergner, J. B., Öberg, K. I., & Rajappan, M. 2019, ApJ, 874, 115
Bock, H., & Mohmand, S. 1977, Angew. Chem. Int. Ed., 89, 105
Bouilloud, M., Fray, N., Bénilan, Y., et al. 2015, MNRAS, 451, 2145
Butscher, T., Duvernay, F., Danger, G., & Chiavassa, T. 2016, A&A, 593, A60
Caselli, P., Hasegawa, T., & Herbst, E. 1993, ApJ, 408, 548
Charnley, S., Tielens, A., & Millar, T. 1992, ApJL, 399, L71
Chuang, K., Fedoseev, G., Qasim, D., et al. 2020, A&A, 635, A199
Dickens, J., Irvine, W. M., Ohishi, M., et al. 1997, ApJ, 489, 753
Dommen, J., Rodler, M., & Ha, T.-K. 1987, CP, 117, 65
Fourikis, N., Sinclair, M., Robinson, B., et al. 1974, AuJPh, 27, 425
Frisch, M., Trucks, G., Schlegel, H., et al. 2009, Gaussian 09, Revision D. 01 (Wallingford, CT: Gaussian)
Haupa, K., Ong, W.-S., & Lee, Y.-P. 2020, PCCP, 22, 6192
Hochstrasser, R., & Wirz, J. 1989, Angew. Chem. Int. Ed., 28, 181
Hochstrasser, R., & Wirz, J. 1990, Angew. Chem. Int. Ed., 29, 411
Hollis, J. M., Pedelty, J., Snyder, L. E., et al. 2003, ApJ, 588, 353
Hovington, P., Drouin, D., & Gauvin, R. 1997, Scanning, 19, 1
Hudson, R. 2018, PCCP, 20, 5389
Hudson, R. L., & Loeffler, M. J. 2013, ApJ, 773, 109
Irvine, W. M., Friberg, P., Kaifu, N., et al. 1989, ApJ, 342, 871
Jamieson, C. S., Mebel, A. M., & Kaiser, R. I. 2006, ApJS, 163, 184
Johansson, L., Andersson, C., Elldér, J., et al. 1984, A&A, 130, 227
Jones, B. M., & Kaiser, R. I. 2013, JPhCh, 4, 1965
Kendall, R. A., Dunning, T. H., Jr., & Harrison, R. J. 1992, JPhCh, 96, 6796
Krim, L., Guillemin, J.-C., & Woon, D. E. 2019, MNRAS, 485, 5210
Lee, C., Yang, W., & Parr, R. G. 1988, PhRvB, 37, 785
Maity, S., Kaiser, R. I., & Jones, B. M. 2014, ApJ, 789, 36
Martin, J. M., & Lee, T. J. 1996, CPL, 258, 136
Matthews, H., & Sears, T. 1986, ApJ, 300, 766
Mehringer, D. M., & Snyder, L. E. 1996, ApJ, 471, 897
Muller, S., Beelen, A., Guélin, M., et al. 2011, A&A, 535, A103
Nummelin, A., Bergman, P., Hjalmarson, Å., et al. 2000, ApJS, 128, 213
Öberg, K. I., Boogert, A. A., Pontoppidan, K. M., et al. 2011, ApJ, 740, 109
Ohishi, M., Kawaguchi, K., Kaifu, N., et al. 1991, in ASP Conf. Ser. 16, Atoms, Ions and Molecules: New Results in Spectral Line Astrophysics (San Francisco, CA: ASP), 387
Peterson, K. A., & Dunning, T. H., Jr. 1995, JPhCh, 102, 2032
Raghavachari, K., Trucks, G. W., Pople, J. A., & Head-Gordon, M. 1989, CPL, 157, 479
Rimola, A., Sodupe, M., & Ugliengo, P. 2012, ApJ, 754, 24
Ruiterkamp, R., Charnley, S., Butner, H., et al. 2007, Ap&SS, 310, 181
Ryazantsev, S. V., Tarroni, R., Feldman, V. I., & Khriachtchev, L. 2017, ChPhC, 18, 949
Scott, A. P., Nobes, R. H., Schaefer, H. F., III, & Radom, L. 1994, JAChS, 116, 10159
Shingledecker, C. N., Álvarez-Barcia, S., Korn, V. H., & Kästner, J. 2019, ApJ, 878, 80
Shivani, Misra, A., & Tandon, P. 2017, RAA, 17, 1
Strazzulla, G., Johnson, R., Newburn, R., et al. 1991, in Comets in the post-Halley Era, ed. R. L. Newburn, Jr. (Dordrecht: Kluwer Academic), 243
Tanaka, K., & Yoshimine, M. 1980, JAChS, 102, 7655
Tucker, K., Kutner, M., & Thaddeus, P. 1974, ApJL, 193, L115
Turner, A. M., Abplanalp, M. J., Blair, T. J., et al. 2018a, ApJS, 234, 6
Turner, A. M., Abplanalp, M. J., Chen, S. Y., et al. 2015, PCCP, 17, 27281
Turner, A. M., Bergantini, A., Abplanalp, M. J., et al. 2018b, NatCo, 9, 3851
Turner, B. 1977, ApJL, 213, L75
Turner, B., Terzieva, R., & Herbst, E. 1999, ApJ, 518, 699
Turner, B. E., & Apponi, A. J. 2001, ApJL, 561, L207
Vacek, G., Galbraith, J. M., Yamaguchi, Y., et al. 1994, JPhCh, 98, 8660
van Baar, B., Weiske, T., Terlouw, J. K., & Schwarz, H. 1986, Angew. Chem. Int. Ed., 25, 282
Vogt, J., Williamson, A. D., & Beauchamp, J. 1978, JAChS, 100, 3478
Werner, H., Knowles, P., Knizia, G., et al. 2015, MOLPRO, v. 2015.1, a Package of ab Initio Programs (Cardiff: University of Cardiff Chemistry Consultants), http://www.molpro.net
Werner, H. J., Knowles, P. J., Knizia, G., et al. 2012, MOLPRO, v. 2012.1, a Package of ab Initio Programs, http://www.molpro.net
Woon, D. E. 2004, AdSpR, 33, 44
Yang, W., Parr, R. G., & Lee, C. 1986, PhRvA, 34, 4586
Zasimov, P. V., Ryazantsev, S. V., Tyurin, D. A., & Feldman, V. I. 2020, MNRAS, 491, 5140
Zhao, L., Kaiser, R. I., Xu, B., et al. 2020, Angew. Chem. Int. Ed., 59, 4051
Zheng, W., Jewitt, D., & Kaiser, R. I. 2006a, ApJ, 639, 534
Zheng, W., Jewitt, D., & Kaiser, R. I. 2006b, ApJ, 648, 753
Zheng, W., Jewitt, D., & Kaiser, R. I. 2007, CPL, 435, 289